# The Structure of Fractal Colloidal Aggregates of Finite Extent

M. Y. LIN,*[,1] R. KLEIN,† H. M. LINDSAY,‡ D. A. WEITZ,§[,2] R. C. BALL[||] AND P. MEAKIN#

*Department of Physics, Princeton University, Princeton, New Jersey 08544; †Fakultat fur Physik, Universitat Konstanz, Konstanz, West Germany; ‡Department of Physics, Emory University, Atlanta, Georgia 30322; §Exxon Research and Engineering Company, Route 22E, Annandale, New Jersey 08801; [||]The Cavendish Laboratory, Madingly Road, Cambridge CB3 9HE, England; and #E. I. DuPont de Nemours Company, Experimental Station, Wilmington, Delaware 19880-0356*

Received September 1, 1989; accepted October 25, 1989

The structure of fractal colloid aggregates formed in both the diffusion- and the reaction-limited regimes is studied by static light scattering experiments. The crossover region of the structure factor of the clusters is measured, and the effects of the finite extent of the fractal structure on the scattering are investigated. The polydispersity of the cluster mass distribution markedly changes the shape of the measured scattering intensity. A form for the structure factor obtained from computer-generated clusters is found to describe the colloidal aggregates very well, for both regimes. Other available models for the crossover region are also discussed. In addition, the effects of the optical plasma resonance in the case of metallic colloids and the effects of cluster restructuring on the static scattering are discussed. 

## I. INTRODUCTION

New insights into the old problem of a quantitative description of colloidal aggregation processes have been obtained in recent years with the recognition that the aggregates are examples of statistical fractal objects (1–4). They can be characterized as mass fractals, meaning that their mass scales with their size $R$ as $M \sim R^{d_f}$, where $d_f$ is the fractal dimension. This simple scaling law applies only above a certain minimal size so that the number of primary colloidal particles in a cluster is sufficiently large. It is also limited at the upper end by the finite size of the clusters. Furthermore, the fractal description of these clusters always implicitly assumes ensemble averaging; for this reason the colloidal aggregates are examples of *statistical* fractals.

Several interrelated properties characterize any aggregation process: The first is the value of the fractal dimension of the clusters, which reflects their geometry. The second is the cluster mass distribution $N(M; t)$, which gives the number of clusters of mass $M$ at time $t$ if the aggregation has been initiated at $t = 0$. A third quantity of importance is the time evolution of the radius of a suitably defined average cluster. These three characteristics of aggregation are intimately related to each other and distinguish the two limiting growth processes of colloid clusters, which have traditionally been called fast and slow aggregation and which are now distinguished as diffusion-limited and reaction-limited cluster aggregation (DLCA and RLCA).

The first significant step in determining these quantities was the quantitative analysis of the transmission electron micrographs of the aggregates (4). This is, however, a cumbersome task, because of the statistical averaging requirements. On the other hand, neutron (5), X-ray (6), and light scattering (7–9) have been used to investigate colloidal aggregates and a proper analysis of these exper-

[1] Present address: National Institute of Standards and Technology, React E151, Gaithersburg, MD 20899.

[2] To whom correspondence should be addressed.



0021-9797/90 $3.00

iments can directly probe the structure of the clusters and determine their fractal dimension. This analysis is rendered difficult by the fact that the measured intensity as a function of the scattering angle is a superposition of the contributions from all clusters within the scattering volume. The experimental results reflect *both* the distribution of different cluster sizes, described by $N(M; t)$ at a time $t$ during the aggregation, *and* the structural correlations of the particles within each cluster. It is the purpose of this paper to present new experimental results on the static light scattering intensity from aggregating colloids for both types of growth processes, DLCA and RLCA, and to analyze these data by properly accounting for the convolution of the cluster mass distributions and the structure of individual clusters. By so doing, we are able to compare the measured structure factor of individual clusters with that predicted theoretically, and thereby determine the form of the cutoff function which describes the boundaries of the fractal clusters and accounts for their finite size.

Starting from the expression for the scattered light intensity from a polydisperse sample, in the next section we examine various analytical expressions for the structure factors, $S_M(q)$, of individual colloidal aggregates of mass $M$ and compare them with results obtained numerically for computer-generated DLCA and RLCA clusters. This knowledge is then used together with the appropriate expressions for the cluster mass distributions for the two regimes of aggregation to analyze the angle dependence of the scattered intensity $I(q)$ in Section III. We show that $I(q)$ is modified appreciably by the cluster mass distribution, $N(M; t)$, which weights the functions $S_M(q)$. Thus, while $S_M(q) \sim q^{-d_f}$ for a small $q^{-1}$ compared to the radius of clusters of mass $M$, $I(q)$ approaches a $q^{-d_f}$ behavior much more slowly. This is not surprising since at any time, $t$, there will be some large clusters for which the structure factor exhibits fractal scaling, $S_M(q) \sim q^{-d_f}$, but there will also be smaller ones, for which $S_M(q)$ has a more complicated $q$ dependence. Therefore, to correctly describe the detailed form of $I(q)$ at different times during the aggregation process requires the proper convolution of the cluster mass distribution, $N(M; t)$, with the structure factor of individual clusters. This provides an experimental test of the functional form of $S_M(q)$.

There are several crucial assumptions which must be made for our analysis, and we confirm their validity in the next two sections. In Section IV we investigate the possibility that multiple scattering of the light precludes the correct determination of $S_M(q)$, and show that this is not the case. In Section V we test the assumption that the clusters can be treated as rigid objects while the experiments are being performed. We report scattering experiments on suspension of DLCA clusters subjected to external shear stress, which can modify the structure of the clusters.

## II. THEORETICAL RESULTS FOR STATIC LIGHT SCATTERING

A static light scattering experiment measures the angle dependence of the scattered intensity which we denote by $I(q)$, where the scattering wavenumber $q$ is related to the scattering angle $\theta$ by $q = (4\pi n/\lambda)\sin(\theta/2)$, with $n$ the refractive index of the solvent and $\lambda$ the wavelength of light *in vacuo*. If $N(M)$ denotes the number of clusters of mass $M$ in the scattering volume and if interactions between the clusters are negligible, the total scattered intensity is given, up to constant factors, by

$$I(q) = \sum_M N(M) I_M(q), \qquad [1]$$

where $I_M(q)$ is the scattered intensity from clusters of mass $M$.

The asymptotic behavior of $I_M(q)$ for large and small $q$ can be obtained from simple, physical arguments. The choice of the scattering angle sets a length scale, given by $q^{-1}$, on which the clusters are probed. This length scale must be compared with a suitably defined length scale of a cluster of mass $M$. Choosing the radius of gyration $R_g$, one may consider

the two limits $qR_g \ll 1$ and $qR_g \gg 1$. In the first case the cluster appears to the light probe essentially as a point particle and thus scatters isotropically, independent of $q$. Since the scattering is completely coherent, the intensity is proportional to $M^2$. Therefore, $I_M(q) \sim M^2$. In the other limit, $qR_g \gg 1$, one may decompose the cluster of radius $R_g$ into smaller subunits or blobs of size $q^{-1}$. As long as the blobs contain many colloidal particles, each blob will be a mass fractal so that the blob mass scales as $m_b \sim (qa)^{-d_f}$, where $a$ denotes the radius for an individual colloidal particle. The phase differences between the scattered fields from particles within a single blob are always less than one. Thus a single blob scatters coherently, and the scattered intensity of the blob will be proportional to $m_b^2$. By contrast, the phase differences between the scattered fields from different blobs are always greater than one. Thus the phases of the electric fields scattered from different blobs add incoherently, and the total intensity will be the sum of the intensities scattered from each blob. The number of blobs in a cluster of mass $M$ is $M/m_b \sim M(qa)^{d_f}$. Therefore, the total scattered intensity is $I_M(q) \sim (M/m_b)m_b^2 \sim M(qa)^{-d_f}$ or $I_M(q) \sim M^2(qR_g)^{-d_f}$.

Since the factor $M^2$ appears in both limiting cases, it is convenient to write $I_M(q) = M^2 S_M(q)$, where $S_M(q)$ denotes the structure factor of clusters of mass $M$. The total scattered intensity, Eq. [1], is therefore given by

$$I(q) = \sum_M N(M)M^2 S_M(q), \qquad [2]$$

which is a measure of both the cluster mass distribution $N(M)$ *and* the form or shape of the clusters.

Although this expression for $I(q)$ looks very simple, in the general case, where $N(M)$ is a broad distribution, $I(q)$ consists of contributions from clusters with $qR_g \gg 1$, from clusters with $qR_g \ll 1$, and from clusters in the crossover region between the two limiting cases. Therefore, caution must be exercised in extracting a value for the fractal dimension $d_f$ from experimental results for $I(q)$ without further knowledge about $N(M)$ and the detailed form of $S_M(q)$ for all values of $qR_g$. For the limiting forms of $S_M(q)$ in Eq. [2] and for the cluster mass distribution obtained experimentally for both DLCA and RLCA, one can find values of the scattering wavenumber for which $I(q)$ is either a constant or varies as $q^{-d_f}$,

$$I(q) = \begin{cases} \sum N(M)M^2 & qR_{max} \ll 1 \\ N_0(qa)^{-d_f} & qR_{min} \gg 1, \end{cases} \qquad [3]$$

where $N_0 = \sum N(M)M$ is the total mass which is constant. The conditions where these limits hold are very stringent: $I(q)$ is strictly independent of $q$ only if $q^{-1}$ is much larger than the radius of the largest cluster $R_{max}$, and the fractal scaling of $I(q)$ is stringly obtained only for $q^{-1}$ much smaller than the radius of the smallest cluster $R_{min}$. As a result of the polydispersity, the crossover from the $q$-independent behavior of the scattered intensity to the fractal scaling regime will, in general, be much broader than the crossover regime of an individual $S_M(q)$. Therefore, for a proper interpretation of scattering experiments, further information is needed about both properties which determine $I(q)$ in Eq. [2]: the structure factor for *all* values of $q$ and the cluster mass distribution $N(M)$.

### *Structure Factor $S_M(q)$*

The structure factor reflects, in $q$ space, the distribution of scattering material in real space; $S_M(q)$ is the Fourier transform of $g(r)$, the density correlation function (10). For a three-dimensional, self-similar object with fractal dimension $d_f$, this function scales as $g(r) \sim r^{d_f-3}$. For colloidal aggregates, however, self-similar scaling occurs only over a limited range of length scales. The upper limit for the scaling form of $g(r)$ occurs when $r$ reaches the radius of gyration, $R_g$. The lower limit of the scaling is given by the radius, $a$, of a primary colloidal particle. This lower limit is not considered here, since lengths of the order of $a$ cannot be resolved in our light scattering ex-

periments. The existence of the upper limit introduces a cutoff function $h(r/R_g)$ such that

$$g_M(r) \sim r^{d_f-3} h(r/R_g), \qquad [4]$$

with $h(v) = 1$ for $v \ll 1$ and $h(v) \to 0$ for $v \gg 1$. Here we attach the index, $M$, to $g_M(r)$ to emphasize that the density correlation function for the cluster depends on the mass, $M \sim R_g^{d_f}$, through the cutoff function.

From Eq. [4] the structure factor is given by

$$S_M(q) \sim \int d^3 r e^{-i\mathbf{q}\cdot\mathbf{r}} g_M(r)$$

$$\sim (qR_g)^{-d_f} f(qR_g), \qquad [5]$$

where

$$f(x) = \int_0^\infty dz z^{d_f-2} h(z/x) \sin z. \qquad [6]$$

As a consequence of the properties of $h(v)$, $f(x) \sim x^{d_f}$ for $x \ll 1$ and $f(x) = \text{const}$ for $x \gg 1$. This ensures that the results in the two limiting cases discussed above are recovered. Furthermore, the shape of the structure factor in the crossover region is described by $f(x)$ in Fourier space of $h(v)$ in real space. Finally, it should be realized that $S_M$ depends on $q$ only through the product $qR_g$, which follows from the fact that $R_g$ is the only relevant length scale of a self-similar cluster with radial symmetry. To emphasize this dependence we will often write $S_M(q) = S(qR_g)$ for the structure factor of clusters of mass $M$.

The detailed shape of $S(qR_g)$, particularly in the regime where $qR_g \gg 1$, depends on the cutoff function, $h(v)$. Several functional forms for $h(v)$ have been suggested and are compiled in Table I. For some simple forms of the cutoff function, the integrals in Eqs. [5] and [6] can be performed analytically. Assuming $h(v) = e^{-\kappa_1 v}$, the structure factor is (11)

$$S(qR_g) = C\left(1 + \frac{q^2 R_g^2}{\kappa_1^2}\right)^{(1-d_f)/2} \times \frac{\sin[(d_f-1)\arctan(qR_g/\kappa_1)]}{(d_f-1)qR_g/\kappa_1}, \qquad [7]$$

TABLE I

Several Proposed Forms for the Cutoff Function

| Model | $h(v)$ $v = r/R_g$ | |
|---|---|---|
| Single exponential | $e^{-\kappa_1 v}$ | |
| Overlapping spheres | $1 - \frac{3}{4}\kappa_2 v + \frac{\kappa_2^3}{16} v^3$ | $v < 2/\kappa_2$ |
| | $0$ | $v > 2/\kappa_2$ |
| Gaussian | $e^{-v^2}$ | |
| Stretched exponential | $e^{-0.2v^{2.5}}$ | |

where $C$ is a constant of order one. Since, according to the definition of the radius of gyration, the structure factor for $qR \ll 1$ must be

$$S(qR_g) = 1 - \frac{1}{3}(qR_g)^2, \qquad [8]$$

the constant $\kappa_1$ is given by $\kappa_1^2 = 3(d_f - 1)/2$. An even simpler structure factor which also fulfills the requirement of Eq. [8] is the modified Fisher–Burford structure factor (12),

$$S(qR_g) = \left(1 + \frac{2}{3d_f} q^2 R_g^2\right)^{-d_f/2}. \qquad [9]$$

Several additional forms for $h(r)$ have also been proposed. Hurd and Flower (13) suggest that $h(v)$ can be described by the overlap volume of two spheres of radius $R_v = R_g/\kappa_2$ separated by the distance $r$. The value of $\kappa_2$, determined from the requirement of Eq. [8], is

$$\kappa_2 = \left(\frac{2d_f(d_f+1)}{(d_f+2)(d_f+5)}\right)^{1/2}. \qquad [10]$$

Another mathematically convenient form for $h(v)$ is a Gaussian (14). Finally, a stretched exponential form based on a fit to the density correlation function of computer-generated clusters has been suggested by Mountain and Mulholland (15). They obtain $h(v) = \exp(-\alpha v^\omega)$ with $\alpha = 0.2$ and $\omega = 2.5$.

In Fig. 1, we plot $g_M(r)$ as a function of the reduced variable $v = r/R_g$ for various models of $h(r)$. The comparison of the results in Fig. 1 shows large differences in the behavior of

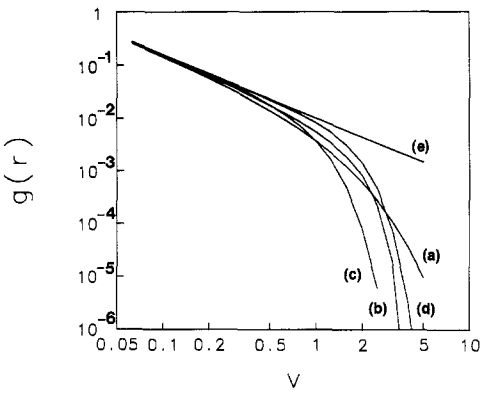


FIG. 1. The pair density correlation function $g(r)$ plotted as a function of $v = r/R_g$ using several different forms for the cutoff function $f(r/R_g)$. (a) Simple exponential, (b) overlapping sphere model, (c) Gaussian, and (d) stretched exponential. Notice how early the curves deviate from the fractal behavior represented by a straight line (e), which does not have a cutoff function.

$g_M(r)$ for the various expressions assumed for $h(v)$. Whereas the results using the simple exponential (a) and the overlapping sphere model (b) start to deviate significantly from the power law behavior (e) at $v \approx 0.1$, the results using the Gaussian (c) and the stretched exponential (d) exhibit a significantly sharper cutoff. This is particularly true for the stretched exponential form. Clearly, the Fourier transform in Eq. [5] will also lead to significantly different shapes for $S(qR_g)$, particularly in the important crossover region, $qR_g \approx 1$.

The stretched exponential form of Mountain and Mulholland suggests that the boundaries of the computer-generated clusters are more sharply defined than predicted by the other forms of $g_M(r)$ discussed above. For this reason we have calculated $S(qR_g)$ directly from computer-generated clusters obtained under diffusion-limited conditions. The simulations provide the positions, $\mathbf{r}_k$, of the particles $k = 1, \ldots, M$ belonging to a cluster of $M$ particles, so that the structure factor can be calculated from

$$S(qR_g) = \frac{1}{M^2}\left\langle \sum_{k,l=1}^{M} \exp[i\mathbf{q}\cdot(\mathbf{r}_k - \mathbf{r}_l)]\right\rangle. \quad [11]$$

The brackets denote an ensemble average which is performed by averaging each cluster over many orientations and by averaging over several clusters having $M$ particles. We use 20 different clusters for each mass, with $M$ extending between 100 and 900. We parameterize the results by fitting to

$$S(x) = \left(1 + \sum_{s=1}^{n} C_s x^{2s}\right)^{-d_f/2n}; \; x = qR_g. \quad [12]$$

This form has the correct limiting behavior of $x \to 0$ and $x \gg 1$. The coefficient $C_1$ is again obtained from the requirement that Eq. [12] must reduce to Eq. [8] for $x \ll 1$; therefore, $C_1 = 2n/3d_f$. We find that we must use $n = 4$ to properly describe the sharp crossover of $S(qR_g)$ around $qR_g \approx 1$. From the fit to the computer-generated DLCA clusters, we obtain $C_2 = 2.50$, $C_3 = -1.52$, $C_4 = 1.02$, and $d_f = 1.8$. We show the results in Fig. 2, where the open circles represent the $S(qR_g)$ calcu-

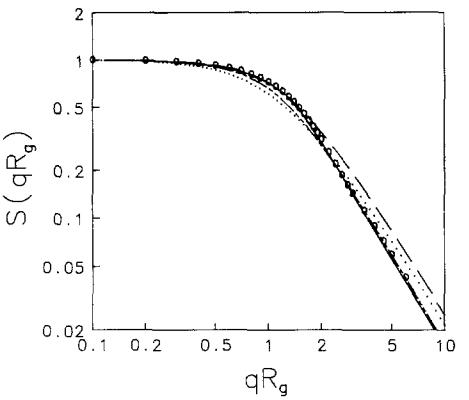


FIG. 2. Various forms of the structure factor for fractal DLCA clusters: the open circles are the results of direct calculation of $S(qR_g)$ using nearly 200 computer-generated DLCA clusters. The solid line is the fit to the expansion form of $S(qR_g)$ in Eq. [12] and agrees well with the simulation over the full range of $qR_g$. The dashed–dotted line uses the stretched exponential form for the cutoff and is very similar to the expansion form. Also shown are structure factors using the exponential (dotted line) and the overlapping sphere (dashed line) cutoff functions. Neither agrees as well with the calculated $S(qR_g)$.

lated from the computer-generated clusters and the solid line is the fit to Eq. [12]. For comparison, we also show the best fits using other forms of $h(v)$. The dashed–dotted line is the stretched exponential cutoff form of Mountain and Mulholland, which is virtually indistinguishable from the fit to Eq. [12]. By contrast, the dashed line is the result of the overlapping sphere cutoff and the dotted line is the result of the exponential cutoff, Eq. [7]; neither form agrees with the calculated $S(qR_g)$ as well as the fit to Eq. [12].

A similar procedure is used to obtain the structure factors for RLCA clusters. We again find it necessary to use $n = 4$; in this case, the value of $d_f = 2.1$ and the coefficients in Eq. [12] are $C_2 = 3.13$, $C_3 = -2.58$, and $C_4 = 0.95$. As in the case of the DLCA aggregates, the fits to the overlapping sphere and exponential forms of the cutoff function yield much poorer agreement with the calculated $S(qR_g)$ for the RLCA clusters than does the polynomial form, while the stretched exponential form provides good agreement.

### *Cluster Mass Distribution N(M)*

The second important function which determines the scattered light intensity, $I(q)$ in Eq. [2], is the cluster mass distribution $N(M)$ or $N(M; t)$, which denotes the number of clusters of mass $M$ in the sample at a time $t$ after the aggregation has been initiated. This function, which reflects the kinetic growth of the clusters, has been studied by employing the Smoluchowski equation (16–18) for irreversible growth and by employing computer simulations (19–21). The Smoluchowski equation is a mean field, balance equation expressing the time rate of change of $N(M; t)$ due to the growth of the clusters. The two different types of aggregation processes; DLCA and RLCA, are reflected in the functional forms of the aggregation kernels $K_{ij}$ which describe the rates at which clusters of mass $M_i$ and $M_j$ merge. Previous investigations have shown that the DLCA growth process can be well approximated with a constant kernel (22–24), for which the Smoluchowski equation can be solved analytically (16), resulting in

$$N(M; t) = \frac{A_1}{M_2(t)}\left(1 - \frac{2}{M_2(t)}\right)^{M-1}, \quad [13]$$

where

$$M_2(t) = \sum_M N(M; t)M^2/N_0. \quad [14]$$

We use the second moment, $M_2$, which is sometimes used to define the "mass of the characteristic cluster." The normalization constant is determined by the requirement that the total mass $N_0$ must be conserved. For RLCA, geometric arguments (18) suggest that the kernel scales as $K_{ij} \sim M_i M_j^{\lambda-1}$ with $\lambda = 1$. This scaling is the same as that of the sum kernel, $K_{ij} \sim M_i + M_j$, for which the Smoluchowski equation can again be solved analytically (16). The RLCA cluster mass distribution has a power-law form with an exponential cutoff at $M_c$ (17),

$$N(M; t) = A_2 M^{-\tau}\exp[-M/M_c(t)], \quad [15]$$

where $\tau = 1.5$. The cutoff mass is simply related to the average mass defined above, $M_c \approx 2M_2$.

A remarkable property exhibited by all solutions to the Smoluchowski equation is dynamic scaling, so that the dependence on aggregation time $t$ only enters through the time dependence of the moments of the distribution (25).

## III. EXPERIMENT AND RESULTS

All of our experiments are performed with charge-stabilized aqueous colloids. Initially, they consist of monodisperse spherical particles at a very low volume fraction. Aggregation is induced by reducing the surface charge or by increasing the concentration of ions in solution, thereby decreasing the screening length. In either case, the repulsive interaction between two approaching particles is reduced (26). Each colloid can be induced to aggregate either rapidly or slowly: by reducing the repulsive barrier to substantially less than $k_BT$,

rapid, diffusion-limited colloid aggregation results; by reducing the repulsive barrier to a few $k_B T$, slow, reaction-limited colloid aggregation results. In both regimes the behavior of each colloid used is identical (27).

In this paper we report experiments using colloidal gold and colloidal silica. The colloidal gold has primary particles of radius $a = 7.5$ nm and an initial volume concentration of $\phi_0 \approx 10^{-6}$. The aggregation is initiated by addition to pyridine, a neutral molecule which adsorbs on the surface of the gold colloids, displacing the surface-adsorbed ions and decreasing the stabilizing charge. The details of the colloid preparation and aggregation for both DLCA and RLCA are described elsewhere (24, 28, 29). The colloidal silica was Ludox-SM obtained from DuPont. The primary particles had a radius of $a = 3.5$ nm and the initial volume fraction was $\phi_0 \approx 10^{-3}$. The silica is initially stabilized by $SiO^-$ groups on the surface. Aggregation was induced by addition of NaCl, which reduces the Debye–Hückel screening and hence the repulsive barrier between the particles.

Colloidal gold has several advantages for these studies. The high scattering cross section helps reduce possible complications due to parasitic scattering from dust or other sources at small angles, allowing signals to be collected when the aggregates are very small. These small aggregates are required to study the crossover region of $I(q)$. Furthermore, these studies require the measurement of $I(q)$ at a single aggregation time $t$ to ensure that the cluster mass distribution is fixed. This is difficult to achieve with an aggregating colloid, particularly for the early stages of DLCA. Fortunately, the aggregation of colloidal gold can be halted by adding a small amount of surfactant to the solution. The surfactant molecules stick to the surface of the gold particles, preventing further aggregation by sterically stabilizing the clusters. The surfactant layer is sufficiently thin that it has no measurable effect on the results. We use the surfactant (30) sodium dodecyl-*o*-xylenesulfonate ($NaC_{12}OXYS$) at a concentration of $10^{-3}$ *M*. All DLCA data were obtained using this method, since the aggregation rate is so fast. For RLCA, the aggregation is substantially slower, lasting from several hours to over a day. Thus measurements from these samples can be obtained while the aggregation progresses.

Our scattering measurements are performed using an $Ar^+$ laser of wavelength $\lambda = 488$ nm. The optical detector is mounted on a goniometer, allowing us to measure the scattering intensity $I(q)$ as function of the scattering angle $\theta$. With an angular scan from $\theta = 10°$ to $\theta = 150°$, a range of $q = 0.003$ nm$^{-1}$ to $q = 0.03$ nm$^{-1}$ is obtained. The goniometer is aligned using the Rayleigh scattering from toluene. We ensure that $I(q)$ measured from toluene is isotropic, independent of $q$, to within fluctuations of $\leq 3\%$. In principle, a wider $q$ range can be achieved by going to smaller angles; in practice, it is difficult to obtain reliable data below 10° with our apparatus.

We show our measurements of $I(q)$ for DLCA gold clusters in a logarithmic plot in Fig. 3a. Four sets of data are plotted to show the evolution of the shape of the scattering with time. The scattering intensity is normalized to the incident power and is corrected for absorption so that the data sets can be compared directly. The linear portion of each data set represents the power-law dependence reflecting the fractal structure of the clusters. At early times, when the clusters are small, the power law behavior is evident only at large $q$. As the clusters grow, the scattering intensity at high $q$ remains unchanged while that at low $q$ increases with time. The power law behavior expands until it ultimately encompasses the entire measurable range of $q$, as shown by the uppermost curve. The fractal dimension $d_f = 1.86$ can be determined directly from the slope of this data set. For this data set, the shape of the cluster mass distribution does not influence the form of $I(q)$, since the majority of the clusters are larger than $q^{-1}$ for all accessible angles. By contrast, the data obtained at earlier aggregation times do not exhibit the linear behavior characteristic of fractal clusters

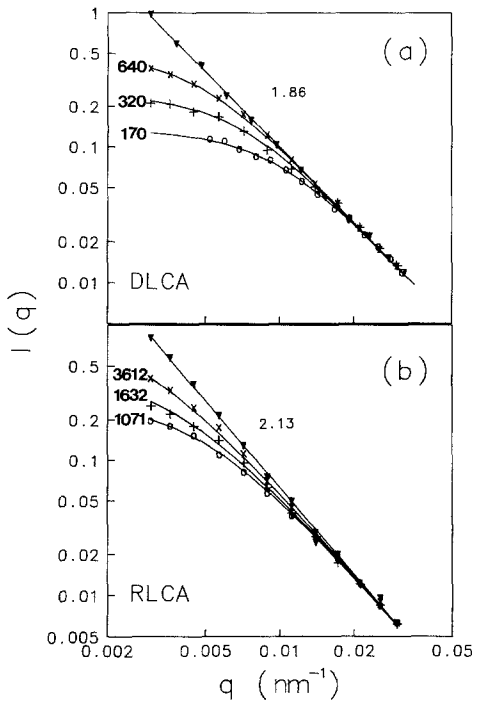


FIG. 3. The scattering intensity $I(q)$ obtained with colloidal gold aggregated by (a) DLCA and (b) RLCA. In each figure, different symbols represent data taken at different aggregation times $t$. The solid curves are the calculations using Eqs. [10]–[14]. The values of $M_2$ obtained in the fitting are labeled with each curve, except the upmost curves, which are linear, giving the fractal dimension $d_f$ = 1.86 for DLCA and $d_f$ = 2.13 for RLCA. $I(q)$ is in arbitrary units.

over all $q$, and the full expression for $I(q)$ in Eq. [2] must be used to describe their shapes. We use the cluster mass distribution given by the solution to the Smoluchowski equation (Eq. [13]), the fractal dimension obtained from the fit to the data at long times, $d_f = 1.86$, and the expansion form of the structure factor for individual clusters, Eq. [12]. The data are fit with Eq. [2], with $M_2(t)$ the only fitting parameter. As can be seen in Fig. 3a, excellent agreement with the shape of the data is obtained. This can provide a method for following the kinetics of the aggregation if sufficient data at the appropriate $q$ range can be collected to allow the determination of $M_2(t)$ as the aggregation progresses. However, this is often difficult, as the limited range of $q$ accessible by light scattering experiments is soon dominated by the scattering of large clusters ($R_g > q^{-1}$), and $I(q)$ is no longer sensitive to $M_2(t)$ in a fit to Eq. [2].

A similar procedure can also be used to describe the RLCA data, as shown in Fig. 3b. In this case, however, a value of $d_f = 2.13$ is determined from the final data set shown, which is obtained at sufficiently long times that the scattering is again dominated by the clusters that are large enough to exhibit power-law $q$ dependence over the full range of wave vectors. For the other three data sets, we use the power-law cluster mass distribution, Eq. [15], and choose $\tau = 1.5$, as has been determined from a scaling analysis of dynamic light scattering data (28). Using the expansion form in Eq. [12] for the structure factor, we fit the data with Eq. [2], where again the only remaining fitting parameter is $M_2(t)$. Excellent agreement with the data is again obtained.

Similar behavior is also observed for other colloids for both diffusion- and reaction-limited colloid aggregation. We have made measurements on silica and polystyrene latex (27); we expect similar results to apply for other colloids irreversibly aggregated in either limiting regime. As an example, in Fig. 4 we show a series of sets of light scattering data from colloidal silica aggregated under RLCA conditions. The aggregation rate was sufficiently slow that $M_2$ changed very little during the

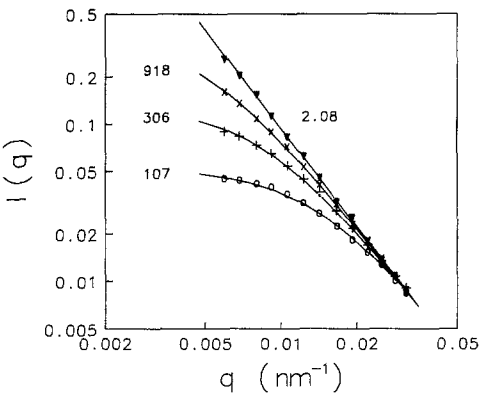


FIG. 4. Scattering intensity $I(q)$ obtained with colloidal silica aggregated by RLCA. It is similar to Fig. 3.

time required to collect a full set of data, which was done as the aggregation proceeded. As can be seen in Fig. 4, the shape of $I(q)$ is identical to the RLCA data from gold in Fig. 3b. The fractal dimension determined from the slope of the final data set is $d_f = 2.08$. Furthermore, excellent fits to the other sets of data are obtained by following the same procedure used for the gold.

Except for the data taken at the longest times, all the results shown in Figs. 3 and 4 are obtained in the crossover region, where the $q$ dependence of the scattering intensity lies between the two asymptotic limits, the isotropic, $q$-independent behavior at $q\bar{R}_g \ll 1$ and the power-law behavior indicative of the fractal structures of the clusters at $q\bar{R}_g \gg 1$. Here we define the radius of the characteristic cluster by $\bar{R}_g = aM_2^{1/d_f}$. The extent in $q$ of this crossover region is indicative of the shape of the cluster mass distribution in each regime. We can set approximate limits on the extent of the crossover regime by estimating where the data become independent of $q$ at small angles and become power law at large angles. For DLCA, this region extends between $0.2 < q\bar{R}_g < 3$, or roughly over one order of magnitude in $q$. By contrast, for the RLCA data, the crossover region extends between $0.02 < q\bar{R}_g < 8$, which is nearly three orders of magnitude in $q$. This difference in extent reflects the different shapes of the cluster mass distributions. For DLCA, the distribution is relatively flat up to the cutoff mass. The additional weighting of $I_M(q) = M^2 S_M(qR_g) \sim M$ for $qR_g > 1$ ensures that the scattering is dominated by the contributions from the largest clusters and the relatively narrow extent of the crossover region reflects this dominance. By contrast, for RLCA, the $M^{-1.5}$ form of the power-law cluster mass distribution greatly mitigates the weighting of $I_M(q)$, so the resultant scattered intensity has important contributions from all clusters. Indeed, if $\tau$ were greater than 2, the scattering intensity would be dominated by the overwhelming number of small clusters (14). Even with $\tau \approx 1.5$, caution must be exercised in extracting the fractal dimension from the scattering data without the inclusion of the consequences of the cluster mass distribution.

The fact that the cluster mass distribution exhibits dynamic scaling and the structure factor is a function of $qR_g$ only also leads to a scaling behavior for the scattered intensity data obtained at different times. The normalized scattering intensity, $I(q)\bar{M}$, is a function of $q\bar{R}$ only, where $\bar{M}(t) = (\bar{R}/a)^{d_f}$ is a moment of the cluster mass distribution $N(M)$. Thus the data obtained at different times can all be scaled onto a single master curve. This scaling is independent of any model and applies to both DLCA and RLCA clusters. Furthermore, the value of $\bar{M}(t)$ required to scale the data onto the master curve can, in principle, be used to follow the kinetics of the aggregation process. However, this scaling procedure can be performed unambiguously only when some curvature due to the finite size of the clusters is observed in the measured $I(q)$. When the measured $I(q)$ exhibits a power-law dependence over the full range of $q$, the value of $\bar{M}(t)$ can no longer be determined unambiguously. Thus the aggregation kinetics can be monitored only at early times. Fortunately, dynamic light scattering data obtained from the aggregation samples also exhibit a scaling behavior which is not limited by the range of $q$ probed (24, 27, 28). In addition, these data obtained with dynamic light scattering can be interpreted using the $S(qR_g)$ and $N(M)$ used here, and the aggregation kinetics can be followed for much longer durations.

The scattering data in the crossover region shown in Figs. 3 and 4 can be used to experimentally test the validity of the various forms that have been proposed for $h(v)$, the cutoff function. This test is best performed using the DLCA data, as the effects of the cluster mass distribution are minimized and the shape of the scattered intensity is more sensitive to $I_M(q)$. In Fig. 5, we show the data set from the gold colloid aggregated by DLCA, where $M_2 = 640$, as shown in Fig. 3a. The solid line in Fig. 5 is the best fit to Eq. [2], using the exponential form for the cutoff function $h(v)$.

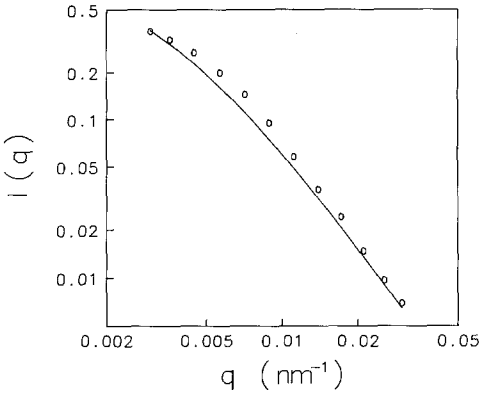


FIG. 5. A trial fit to the scattering intensity $I(q)$ (squares) using the exponential cutoff function. As can be seen, the calculations do not fit the data very well. The data are from DLCA gold clusters, shown in Fig. 3a with $M_2$ = 640.

The DLCA form of the cluster mass distribution (Eq. [13]) is used, with $M_2$ the only adjustable parameter. As can be seen, the agreement with the data is markedly poorer than that for the structure obtained from the computer-generated DLCA clusters, Eq. [12]. Similarly, poor agreement is also found using the overlapping sphere, the modified Fisher–Burford, and the Gaussian forms of the cutoff function. By contrast, a good fit is obtained using the stretched exponential cutoff of Mountain and Mulholland, as should be expected from the behavior of the structure factors shown in Fig. 2. Similar results are also obtained for the RLCA clusters: the expansion form for the structure factor and the stretched exponential cutoff function, both obtained as fits to computer-generated clusters, give considerably better agreement with the data than the other forms of the cutoff function. However, these differences are less pronounced for the RLCA data than for the DLCA data because the increased polydispersity in the cluster mass distribution smears out, to some extent, the differences between the various forms of the structure factor.

Physically, the origin of the discrepancy between the different forms of the cutoff functions arises from the sharpness of the cutoff of the correlation functions around $R_g$. This cutoff for the computer-simulated clusters is much sharper than those for all the analytical forms for $h(v)$ except the stretched exponential. The remarkable agreement between the computer simulations and the data demonstrates that the structure of the clusters predicted by the simulations is in fact very similar to that of the clusters formed in experiment. This is one of the most critical tests confirming the veracity of the computer simulations of aggregation.

In fitting each set of data, we have assumed that the cluster mass distribution is that given by the solution to the Smoluchowski equation. However, the actual fits to the data cannot determine the cluster mass distribution $N(M)$ unambiguously. This is particularly true for the RLCA regime, where $N(M)$ depends on two parameters, $M_2(t)$ and $\tau$. Equally good fits are obtained for the RLCA data using different values of the cluster mass exponent, $\tau$. A more sensitive test of the forms used for $N(M)$ is provided by the scaling of dynamic light scattering data. This confirms (27, 28) the choice for $N(M)$ used here and determines the value of $\tau$ = 1.5. However, the essential conclusion of the validity of $S_M(qR_g)$ obtained from the computer-generated clusters is independent of the details of the $N(M)$ chosen.

Finally, we note that the intensity data can also be represented by an effective structure factor, which includes the smearing due to the polydispersity of the cluster mass distribution, $I(q) \sim M_2^2 S_{\text{eff}}(q\bar{R}_g)$. However, because of the nontrivial dependence on the polydispersity, the quantity $\bar{R}_g$ thus obtained lacks a well-defined physical meaning. In addition, it is only when data can be collected at sufficiently small $q$, where $I(q)$ is independent of $q$, that the characteristic mass, $M_2$, can be determined directly.

## IV. TESTS FOR MULTIPLE SCATTERING

The optical properties of the gold aggregates are unique among the colloids used here in that they are influenced by the plasma resonance that is characteristic of small metallic

particles (29, 31, 32). This plasma resonance leads to a large increase in the optical absorption of the colloidal gold with a concomitant increase in the scattering intensity. The consequences of this plasma resonance on the optical properties of gold particles have led to some confusion in the literature, and recent reports by Wilcoxon *et al.* (33, 34) have claimed static light scattering cannot be used to measure $d_f$ for colloidal gold aggregates because of the influence of multiple scattering. If this were indeed true, the measured static scattering would not accurately reflect the structure factor of the aggregates and their fractal correlations, invalidating much of our interpretation of the data for the case of gold. In this section we investigate the independence of the static scattering from the gold aggregates as the excitation wavelength is varied closer to the optical resonance and as the concentration of the clusters is varied and show that the results are *not* influenced by multiple scattering.

The optical plasma resonance of small metallic particles arises from the collective excitation of the electrons in the metal, which leads to a large increase in the polarizability of the particles. The behavior of the plasma resonance depends on both the shape of the particles and their local environment. Thus the frequency and the strength of the resonance is modified when the particles are aggregated. As a result of the plasma resonance, the scattering from the gold aggregates is several orders of magnitude larger than that from silica or polystyrene aggregates of comparable size. In addition, there is a pronounced wavelength dependence of the scattering intensity. However, the $q$ dependence of the static light scattering still accurately reflects the fractal structure of the clusters (32).

All of the results reported above were obtained using $\lambda = 488$ nm, which is well away from the measured resonance of the gold clusters, occurring at about 740 nm. The most convincing experimental evidence that multiple scattering does not affect the results is the fact that the static light scattering from the gold aggregates behaves in *exactly* the same way as that from the silica and polystyrene aggregates (27), whose intrinsic scattering is roughly two to three orders of magnitude less than the gold. The $q$ dependence of $I(q)$ from large aggregates is the same for all three colloids, and the fractal dimensions determined from the slopes of the scattering are identical to within experimental error, for both the DLCA and the RLCA clusters. In addition, the scattering from smaller aggregates of gold behaves in the same fashion as that from the silica aggregates, as illustrated by Figs. 3b and 4. Thus, at least for $\lambda = 488$ nm, multiple scattering cannot affect the results.

The possibility that multiple scattering obcures the fractal correlations in the $q$ dependence of the scattering intensity from a single cluster has been considered theoretically by Chen *et al.* (35). They used computer-generated clusters to numerically calculate the local electric field at each particle, and included, in a self-consistent fashion, the contributions of both the applied field and the radiated field from all the other particles that constitute the cluster. Using optical constants suitable for gold clusters, they found that the electric field at each particle has a large, but random and fluctuating, local field correction. However, this does not modify the angle dependence of the scattering, and the $q^{-d_f}$ behavior at large $q$ is preserved. Physically, the origin of this can be understood to result from the random nature of the local field corrections at each particle. Since the scattered intensity at any value of $q$ is a correlation of the fields contributed from particles at *different* positions, only those components of the field that are correlated will make a contribution. Thus, the scattering of the applied field exhibits the fractal correlations due to the structure of the cluster. In addition, the scattering from the average contribution of the local fields, which is the same at all particles, contributes to the fractal correlations and can be viewed as reflecting the average refractive index due to the particles in the cluster. By contrast, the fluctuating portion of the field is random and po-

sesses no spatial correlations. Thus the scattering from this portion of the local field cannot contribute to the fractal correlations and the resultant $q^{-d_f}$ dependence of the scattering intensity. Instead, it simply provides a constant, isotropic contribution to the scattering intensity, which is independent of $q$. However, even at the largest $q$ probed in the experiments, this contribution is at least two orders of magnitude smaller than the $q^{-d_f}$-dependent contribution due to the fractal correlations (35). Thus the overall $q$ dependence is unchanged on the logarithmic plots and, in particular, the slope remains $-d_f$.

We can also investigate the effects of the optical plasma resonance experimentally by measuring $I(q)$ as the excitation wavelength is varied. We use a gold colloid aggregated under DLCA conditions using pyridine as the initiator. The aggregation was stopped by adding surfactant, and the scattering intensity, $I(q)$, was measured using different laser wavelengths for the excitation. In the upper part of Fig. 6, we compare the data obtained with $\lambda$ = 488 nm (b) to those obtained with $\lambda$ = 633 nm (a) using a HeNe laser to approach the peak of the adsorption resonance.

The solid line through the data obtained with $\lambda$ = 488 nm is a fit to the asymptotic form of $I(q)$ for large clusters, and gives $d_f$ = 1.84. A solid line with the same slope is also drawn through the data obtained at $\lambda$ = 633 nm. It follows the data perfectly, except for the three data points at the highest $q$, which display a slight but noticeable deviation, curving upward from the solid line. This "tail" at high $q$ results from the effects of the optical plasma resonance, and its origin is discussed elsewhere (36). The tail does not result from multiple scattering, as it occurs at high $q$, where the scattering is the weakest, rather than at low $q$, where it is the strongest. However, since fractal correlations lead to a linear behavior on a logarithmic plot, and since the data at the highest $q$ obtained with $\lambda$ = 633 nm are clearly not linear, their contribution should not be included in determining the fractal dimension from the data. A fit to the data below $q$ = 0.02 nm$^{-1}$ gives a fractal dimension identical to that determined from the data obtained at $\lambda$ = 488 nm.

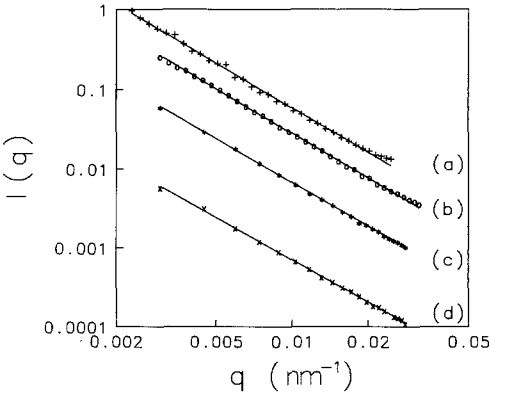


FIG. 6. Static light scattering (in arbitrary units) from DLCA gold aggregates obtained from the same sample with excitation using (a) 633 nm and (b) 488 nm. While the intensity of the overall scattering at 633 nm increases due to the plasma resonance, the shape of $I(q)$ is unchanged, except for the three data points at the highest $q$. Also shown are data obtained from the same samples using $\lambda$ = 488 nm (c) before and (d) after dilution by a factor of 10. The dilution was performed sufficiently gently to eliminate restructuring the aggregates. The measured shape of $I(q)$ is unchanged. All these data are normalized to the incident power and corrected for absorption, but data sets (b) and (c) are offset for clarity. These data demonstrate *conclusively* that multiple scattering, from either single clusters or cluster concentration, does not affect the determination of $d_f$ from $I(q)$.

Similar effects are also observed for aggregates formed under RLCA conditions (8). Here, in fact, the deviation from the linear behavior at high $q$ for $\lambda$ = 633 nm excitation is somewhat more apparent, since the slope of the linear region is higher.

In a recent paper, Wilcoxon *et al.* (34) have suggested that the slope of $I(q)$ from gold aggregates varies as the excitation wavelength is varied. However, they base their conclusion on a fit of their data to a single linear behavior, over the whole range of $q$ measured. Closer examination of their published data shows that it exhibits the same behavior as those reported here: there is a distinct curvature at the highest $q$, which becomes more apparent as $\lambda$ approaches the absorption resonance. However,

if the linear region of their data at different wavelengths is compared, the correct result of a wavelength-independent $d_f$ is recovered. Fitting the whole set of data to a single power law, without allowing for possible deviations, causes the measured slope of the data to decrease as the exciting wavelength is varied. Doing so, however, is analogous to fitting the data obtained at earlier times from smaller clusters to a single power law. In either case, essential physics is obscured.

The results discussed above show that multiple scattering of the light within individual clusters does not affect our conclusions. We can also consider the possibility that multiple scattering results from the concentration of clusters in solution. To do so, we compare the scattering from a solution at full concentration to that obtained from a solution whose concentration has been reduced by a factor of 10. However, to make this comparison convincing, it is essential to use the same colloid solution, to avoid the sample to sample variations in the scattering that typically arise and can cause a change in the fractal dimension, determined from the slope of the scattering to be roughly $\pm 0.1$. In performing the dilution, it is also essential that the amount of shear induced by the mixing be minimized, to avoid the problem of restructuring the delicate fractal clusters, as is discussed in more detail in the next section.

Thus we first prepare a sample of DLCA clusters, stop the aggregation by adding surfactant, and then measure the scattering. Next the sample is diluted by a factor of 10 by gently pouring water down the side of the scattering cell, ensuring mixing with minimal shear. The scattering is then measured from the diluted solution of the same sample. The data are shown in Figs. 6c and 6d. As can be seen, the results are indistinguishable, and there is no change whatsoever in the $q$ dependence of the scattering upon dilution. Thus we conclude that multiple scattering does not occur from the gold aggregates as these values of initial particle concentration.

Again, Wilcoxon *et al.* have arrived at a different conclusion. However, in one experiment (33), they clearly caused a restructuring of the clusters when they diluted the sample, as the scattering they report is identical in shape to the scattering obtained from clusters subjected to small amounts of shear with or without dilution (37), as reported in the next section. In a second experiment (34), they compared the scattering from different samples which were first diluted and then aggregated. While this procedure clearly avoids the potential of restructuring, the samples compared are no longer identical. This latter problem is further exacerbated by the fact that the diluted colloid, which has a much smaller ratio of surface area to volume, is much more susceptible to the effects of impurities. Indeed, our own experience suggests that the problem of sample cleanliness, required to obtain consistent and reproducible results, is much more severe at lower concentrations. Thus, the variations that Wilcoxon *et al.* observe are most likely due to the sample to sample variations. The variations are clearly not due to multiple scattering, since, as shown above, the scattering is unchanged if the same sample is used.

In conclusion, we note that the strongest evidence that the gold colloids do not exhibit multiple scattering is the fact that their behavior is identical to that obtained from dielectric colloids whose scattering intensity is about three orders of magnitude less. We find no evidence whatsoever to support the claims of Wilcoxon *et al.* and instead find that their observations can be interpreted in a simple manner that does not involve multiple scattering. Thus, we conclude that the optical plasma resonance does not obscure the effects of the fractal correlations in $I(q)$, and the light scattering from colloidal gold can be interpreted in the manner presented in this paper.

## V. RESTRUCTURING OF FRACTAL AGGREGATES

Since the fractal dimension of colloid aggregates is around $d_f \sim 2$, they are rather tenuous objects. As such, we might expect them

to be quite fragile and very susceptible to deformation. Indeed, silica DLCA aggregates have been found to undergo spontaneous restructuring in some cases (38). Furthermore, a recent calculation (39) of the mechanical properties of colloidal aggregates showed that the fractal structure can persist only up to some critical size, whereupon they become unstable to either thermal fluctuations or gravitational distortion. The previous interpretation of the static light scattering data, and also of the quasielastic scattering experiments reported elsewhere, rests upon the assumption of rigid fractal objects. It is therefore important to test this assumption, for instance, by deliberately exposing the clusters to external forces. In this section, we exploit our knowledge of the static light scattering from fractal aggregates to study the mechanical properties of the clusters. To obtain controllable and reproducible results, we study the effects of an external shear stress on the structure of the aggregates. These effects are of importance to ensure that our interpretation of static light scattering is not biased by cluster restructuring. In addition, they are of technological importance in determining the physical properties of fractal materials, which are produced by numerous random growth processes.

Neither thermal fluctuations nor gravity has been found to cause deformation of the fractal structure of the colloidal gold aggregates when their size is sufficiently small to avoid sedimentation. Thus, to controllably deform them, we apply an external shear stress. This is done by forcing the clusters to flow through a narrow tube at different flow rates. We characterize the degree of shear by the maximum shear stress applied, $\sigma_m$, which depends on the tube radius, $b$, and the flow rate, $\Phi$,

$$\sigma_m = \gamma\eta = \frac{4\Phi\eta}{\pi b^3}, \qquad [16]$$

where $\gamma$ denotes the shear rate and $\eta$ is the viscosity. Through the use of a very short length of tube, the clusters are exposed to the shear for times shorter than ~0.5 s, ensuring that no significant aggregation occurs during the shearing. The aggregates are forced through the tube using a syringe pump, allowing the maximum shear stress to be varied by changing the flow rate. Immediately after the shearing, the aggregation is stopped by addition of surfactant. We use aggregates formed by DLCA to reduce the effects of polydispersity in the light scattering and to have more tenuous clusters, which should be more susceptible to shear-induced deformation.

The clusters are aggregated until the characteristic cluster radius is roughly 500 nm, as measured by dynamic light scattering, and then the shear is applied. The $q$ dependence of the scattering intensity is measured and compared with that obtained from the same colloid not subjected to shear. We show examples of the results obtained in Fig. 7. The lowest curve is obtained from the unsheared aggregates and exhibits the expected linear behavior, giving a fractal dimension of $d_f = 1.84$, as shown by the solid line, which is a fit to the data. The upper three curves are the scattering from aggregates subjected to increasing amounts of shear stress, 200, 290, and 580

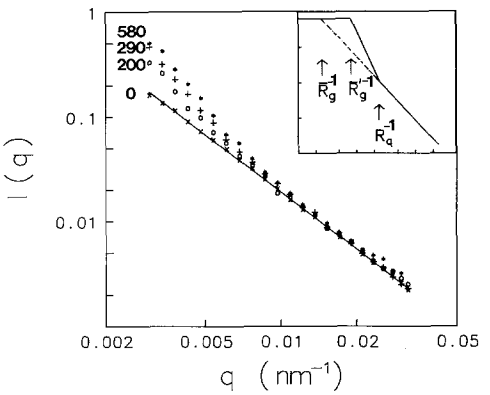


FIG. 7. A logarithmic plot of the scattering intensity from DLCA gold clusters before and after being subjected to varying amounts of shear. The maximum shear stress applied is labeled beside each data set. The data (×) obtained from aggregates not subjected to shear exhibit linear behavior with a slope giving $d_f = 1.84$. The shear causes restructuring of the fractal shape, changing the slope of the scattering at low $q$. The inset shows schematically the expected effect of the restructuring on the scattering.

dyn/cm$^2$. They no longer exhibit a simple, linear shape. Instead, there is a distinct kink in each curve which occurs at successively larger values of $q$ as the maximum shear stress is increased. At small $q$ the slope of the scattering increases markedly with increasing shear, although it is not really possible to describe it as linear on the logarithmic plot given the limited range of $q$ probed. By contrast, at large $q$ the scattering still has the same slope as that from unsheared clusters, and, indeed, is indistinguishable from the unsheared clusters.

These changes in the shape of the scattered intensity show that some restructuring of the tenuous fractal clusters has occurred. A plausible physical picture is that the shear causes the fractal aggregates to bend or deform, resulting in the formation of loops and additional bonds, leading to a strengthening of the structure. These loops would tend to be formed on larger length scales, where the structure is weaker and the forces larger. The formation of the loops at these larger length scales would modify the fractal correlations, and would, in fact, tend to decrease the tenuousness of the clusters, leading to an apparent increase in the fractal dimension. However, below some length scale, the aggregates are strong enough to withstand the shear to which they are subjected, and the fractal correlations persist.

Another possible interpretation of the results is that the shear causes the clusters to break apart, with the weaker arms falling off. However, using dynamic light scattering to measure the average hydrodynamic radius, we do not see any measurable change in $\bar{R}_h$ after the shear is applied. Further evidence suggesting that the clusters are not broken apart comes from experiments where surfactant was added to arrest the aggregation before shear was applied. In this case no changes in the static scattering could be detected. The effect of adding the surfactant is to prevent the gold particles from sticking to each other when their distance becomes very small. We speculate that whereas the addition of surfactant will not influence the possibility of breaking the clusters, the formation of additional loops is prevented by the surfactant coating. Although an arm might be bent under the application of shear and might touch another part of the cluster, these two parts will not stick together when sterically stabilized by the surfactant coating, so that after the removal of the applied stress, the cluster will regain a shape which is not too different from the one it had before the application of shear.

The restructuring of the fractal clusters clearly will affect the shape of the scattered intensity. While the detailed shape of $I(q)$ has yet to be determined, a qualitative picture of the consequences of the restructuring is represented schematically in the inset of Fig. 7. The lower, dashed curve represents the scattering prior to the application of the shear. The linear region reflects the fractal structure of the clusters, with a slope of $-d_f$. Then, at low $q$, when $q < \bar{R}_g^{-1}$, the scattering is isotropic, independent of $q$. A sharp crossover is shown here, although, of course, it is in practice considerably broader. The scattering from the restructured clusters is shown by the upper, solid curve. The formation of loops and additional bonds will ensure that some of the mass of the clusters is moved toward their centers, then decreasing $\bar{R}_g$. Thus the isotropic scattering will extend to larger $q$, until $q \sim \bar{R}_g'^{-1}$. However, since the fractal structure is sufficiently robust at short length scales that it is not deformed, the scattering at large $q$ must remain unchanged. If the characteristic length scale below which the structure is unchanged is $R_q$, then the scattering is unaffected for $q > R_q^{-1}$. Between the two limits, for $\bar{R}_g'^{-1} < q < R_q^{-1}$, the scattered intensity must smoothly join the two extremes. As shown in the inset of Fig. 7, one way to achieve this is by a power-law dependence, $I(q) \sim q^{-s}$. Now, however, since $\bar{R}_g' < \bar{R}_g$, we must have $s > d_f$, so that the apparent slope increases. We note, however, that there is no intrinsic requirement for a power-law dependence, and thus the slope, $s$, has no special meaning. This description of the scattered intensity accounts for the

observed behavior very well. Nevertheless, we emphasize that it is only a qualitative description, one that should be verified through computer simulation of both the restructuring and the resultant $I(q)$.

While we cannot conclusively verify the validity of this picture of the restructuring and resultant changes in the scattering, we can investigate some of the consequences. One consequence of this picture is that the degree of restructuring should depend on the initial size of the cluster $R_g$, as well as on the magnitude of the shear applied. To quantify these effects, we parameterize the consequences of the shear in two ways: first, we measure the asymptotic slopes of the scattered intensity at both small and large $q$; and second, we determine the crossover radius $R_q$, given by the inverse of the value of $q$, where the two slopes intercept (see inset to Fig. 7).

The crossover radius, $R_q$, determines the spatial extent of the restructuring. At length scales smaller than $R_q$, the fractal structure is sufficiently robust that it does not undergo any restructuring. At larger length scales the tenuous structure of clusters is modified, changing the shape of the scattering at low $q$. The apparent slope of this low $q$ scattering measures the degree of restructuring. We expect that, as the shear stress is increased, the clusters will undergo more restructuring, which will result in a decrease in this new radius of gyration, $\bar{R}_g'$. If $\bar{R}_g'$ decreases more rapidly than $R_q$, then the exponent $s$ will have to increase as well.

The results of this investigation are shown in Fig. 8, where we plot both $s$ and $R_q$ as functions of the maximum shear stress for two different sets of DLCA clusters, with sizes $\bar{R}_g \approx 1000$ nm and $\bar{R}_g \approx 500$ nm. As shown in Fig. 8a, we find that $R_q$ decreases very rapidly with increasing shear, but then seems to approach a constant, asymptotic value of $R_q \approx 100$ nm for all values of shear stress achieved in our experiments. Within the accuracy of these measurements, both sets of clusters appear to be affected up to the same limiting value of $R_q$. By contrast, there is a

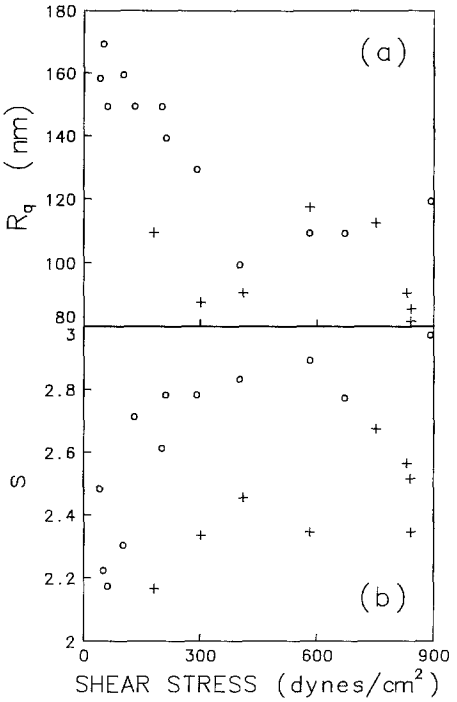


FIG. 8. The effects of applied shear stress on DLCA gold clusters as seen in the static light scattering: (a) the crossover radius, and (b) $s$, the slope at low $q$, both measured from the scattering data plots similar to Fig. 6. In both figures, the squares are for clusters with a characteristic radius $\bar{R} \approx 500$ nm, and the pluses are for clusters with $\bar{R} \approx 210$ nm.

distinct difference in the behavior of $s$ for each set of clusters, as shown in Fig. 8b. In both cases, $s$ is considerably greater than $d_f = 1.84$ for all values of shear stress used. Furthermore, the high $q$ scattering in all cases was unchanged and had the same slope, giving $d_f \approx 1.84$. However, for all values of the shear stress, the larger clusters have a larger value of $s$ than the smaller clusters. The values of $s$ may also reach an asymptotic limit at high shear, although the scatter in the data prevents an accurate determination of its value. Our experiments show that a certain finite shear stress must be applied to introduce a detectable effect on the structure of the aggregates. From this result, it can be concluded that the experiments on unsheared samples can be interpreted by as-

suming the clusters to be rigid objects. However, the handling of the samples during the experiments, such as diluting them and turning the tubes to avoid sedimentation effects, must be done with great care.

Finally, we note that Wilcoxon *et al.* (34) have suggested that shear does not modify the structure of the clusters. Instead, they simply draw a single power-law fit through the data obtained from the sheared samples. Not surprisingly, they find that the slope increases from the unsheared sample. However, this procedure was carried out by replotting previously published data of Lindsay *et al.* (32) with a claim that the increase in the slope reflects the sample to sample fluctuations of the data. Needless to say, their fit to the sheared data is substantially worse than their fit to the unsheared data. In addition, it is difficult to reconcile their interpretation with the clear trend exhibited by the data shown in Fig. 7, where the changes with increased shear are apparent. Thus we believe that the interpretation by Wilcoxon *et al.* should be discarded. Their interpretation can be attributed to the fact that they reinterpreted only a limited amount of previously published data. They did not provide any new experimental data.

## VI. CONCLUSIONS

The analysis of static light scattering from colloidal aggregates presented in this paper shows the importance of the cluster mass distribution for a quantitative understanding of $I(q)$. Whereas the $q$ dependence of the structure factors $S_M(q)$ of clusters of mass $M$ exhibits a remarkably sharp crossover from the $q$-independent behavior at small $q$ to the fractal scaling for large $q$, this transition region is significantly broader for the measured light scattering intensity, $I(q)$, due to the polydispersity introduced by the cluster mass distribution, $N(M; t)$. This is particularly pronounced for the case of reaction-limited colloid aggregation due to the power-law dependence of the cluster mass distribution.

This conclusion has been reached by combining results for the structure factors $S_M(q)$ from computer-generated clusters with analytic expressions for the cluster mass distribution obtained from the Smoluchowski equation for irreversible growth. The experimental results for $I(q)$ can be quantitatively described for both limiting regimes of cluster aggregation, DLCA and RLCA. We find that the computer-generated $S_M(qR_g)$ provides a remarkably good description of the shape of the clusters, including the cutoff describing their finite extent. By contrast, other suggested forms for this cutoff do not describe the data as well.

Given this understanding of static light scattering, we have used this technique to study colloidal aggregates subjected to an external shear stress. Whereas the clusters are restructured at large length scales, they are found to maintain their original fractal correlations at small lengths.

## REFERENCES

1. Meakin, P., *in* "Phase Transitions and Critical Phenomena" (C. Domb and J. L. Lebowitz, Eds.), Vol. 12, p. 335. Academic Press, New York, 1988.
2. Family, F., and Landau, D. P., (Eds.), "Kinetic Aggregation and Gelation." Elsevier, Amsterdam, 1984.
3. Weitz, D. A., Lin, M. Y., and Huang, J. S., *in* "Physics of Complex and Supermolecular Fluids" (S. A. Safran and N. A. Clark, Eds.), p. 509. Wiley–Interscience, New York, 1987.
4. Weitz, D. A., and Oliveria, M., *Phys. Rev. Lett.* **52,** 1433 (1984).
5. Weitz, D. A., Lin, M. Y., Huang, J. S., Witten, T. A., Sinha, S. K., Gethner, J. S., and Ball, R. C., *in* "Scaling Phenomena in Disordered Systems" (R. Pynn and A. Skjeltorp, Eds.), p. 171. Plenum, New York, 1985.
6. Dimon, P., Sinha, S. K., Weitz, D. A., Safinya, C. R., Smith, G. S., Varady, W. A., and Lindsay, H. M., *Phys. Rev. Lett.* **57,** 595 (1986).
7. Schaefer, D. W., Martin, J. E., Wiltzius, P., and Cannell, D. S., *Phys. Rev. Lett.* **52,** 2371 (1984).
8. Weitz, D. A., Huang, J. S., Lin, M. Y., and Sung, J., *Phys. Rev. Lett.* **54,** 1416 (1985).
9. Matsushita, M., Hayakawa, Y., Sumida, K., and Sawada, Y., *in* "Proceedings of the First International Conference for Science on Form" (S. Ishizaka,

Ed.), p. 23. KTK Scientific Publishers, Tokyo, 1986.
10. We assume that there are no correlations between the clusters themselves. If such correlations did exist, it would be more appropriate to refer to $S_M(q)$ as the form factor of the clusters and to reserve the use of the structure factor to represent the correlations between different clusters.
11. Freltoft, T., Kjems, J. K., and Sinha, S. K., *Phys. Rev. B* **33,** 269 (1986).
12. Dietler, G., Aubert, C., Cannell, D. S., and Wiltzius, P., *Phys. Rev. Lett.* **57,** 3117 (1986).
13. Hurd, A. J., and Flower, W. L., *J. Colloid Interface Sci.* **122,** 178 (1988).
14. Martin, J. E., and Ackerson, B. J., *Phys. Rev. A* **31,** 1180 (1985).
15. Mountain, R. G., and Mulholland, G. W., *Langmuir* **4,** 1321 (1988).
16. Cohen, R. J., and Benedek, G. B., *J. Phys. Chem.* **86,** 3696 (1982).
17. Von Dongen, G. J., and Ernst, M. H., *Phys. Rev. Lett.* **54,** 1396 (1985).
18. Ball, R. C., Weitz, D. A., Witten, T. A., and Layvraz, F., *Phys. Rev. Lett.* **58,** 274 (1985).
19. Meakin, P., *Adv. Colloid Interface Sci.* **28,** 249 (1988).
20. Meakin, P., and Family, F., *Phys. Rev. A* **36,** 5498 (1987).
21. Brown, W. D., and Ball, R. C., *J. Phys. A* **18,** L517 (1985).
22. Weitz, D. A., and Lin, M. Y., *Phys. Rev. Lett.* **57,** 2037 (1986).
23. Lindsay, H. M., Lin, M. Y., Weitz, D. A., Ball, R. C., Klein, R., and Meakin, P., *in* "Proceedings, Photon Correlation Techniques and Applications," Vol. 1, p. 122. OSA, Washington, DC, 1988.
24. Lin, M. Y., Lindsay, H. M., Weitz, D. A., Klein, R., Ball, R. C., and Meakin, P., *J. Phys. Condens. Matter* **2,** 3093 (1990).
25. Vicsek, T., and Family, F., *Phys. Rev. Lett.* **52,** 1669 (1984).
26. Verwey, E. J. W., and Overbeek, J. T. G., "Theory of the Stability of Lyophobic Colloids." Elsevier, Amsterdam, 1948.
27. Lin, M. Y., Lindsay, H. M., Weitz, D. A. Ball, R. C. Klein, and Meakin, P., *Nature (London)* **339,** 360 (1989).
28. Lin, M. Y., Lindsay, H. M., Weitz, D. A., Ball, R. C., Klein, R., and Meakin, P., *Phys. Rev. A* **41,** 2005 (1990)
29. Weitz, D. A., Lin, M. Y., and Sandroff, C. J., *Surf. Sci.* **158,** 147 (1985).
30. Sheu, E. Y., Chen, S. H., and Huang, J. S., *J. Phys. Chem.* **91,** 1535 (1987).
31. Kerker, M., "The Scattering of Light." Academic Press, New York, 1969.
32. Lindsay, H. M., Lin, M. Y., Weitz, D. A., Sheng, P., Chen, Z., Klein, R., and Meakin, P., *Faraday Discuss. Chem. Soc.* **83,** 153 (1987).
33. Wilcoxon, J. P., Martin, J. E., and Schaefer, D. W., *Phys. Rev. Lett.* **58,** 1051 (1987).
34. Wilcoxon, J. P., Martin, J. E., and Schaefer, D. W., *Phys. Rev. A* **39,** 2675 (1989).
35. Chen, Z., Sheng, P., Weitz, D. A., Lindsay, M. Y., and Meakin, P., *Phys. Rev. B* **37,** 5232 (1988).
36. Sheng, P., Chen, Z., Weitz, D. A., and Lin, M. Y., to be published.
37. Weitz, D. A., Lin, M. Y., Lindsay, H. M., and Huang, J. S., *Phys. Rev. Lett.* **58,** 1052 (1987).
38. Aubert, C., and Cannell, D. S., *Phys. Rev. Lett.* **56,** 738 (1986).
39. Kantor, Y., and Witten, T. A., *J. Phys. Lett.* **45,** L675 (1984).